ACS OMEGA

Article

http://pubs.acs.org/journal/acsodf

Electrochemical and SECM Investigation of MoS_2/GO and MoS_2/rGO Nanocomposite Materials for HER Electrocatalysis

Sriram Kumar,[†,‡] Prasanta Kumar Sahoo,[§] and Ashis Kumar Satpati*[,†,‡]

[†]Analytical Chemistry Division, Bhabha Atomic Research Centre, Trombay, Mumbai 400085, India

[‡]Homi Bhabha National Institute, Anushaktinagar, Mumbai 400094, India

[§]Centre for Nano Science and Nano Technology, Siksha 'O' Anusandhan University, Bhubaneswar 751030, Odisha, India

Supporting Information

ABSTRACT: Development of advanced materials for electrocatalytic and photocatalytic water splitting is the key in utilization of renewable energy. In the present work, we have synthesized MoS_2 nanoparticles embedded over the graphene oxide (GO) and reduced graphene oxide (rGO) layer for superior catalytic activity in the hydrogen evolution process (HER). The nanocomposite materials are characterized using different spectroscopic and microscopic measurements. A Tafel slope of ~40 mV/decade suggested the Volmer–Heyrovsky mechanism for the HER process with MoS_2/GO composite as the catalyst, which indicated that electrochemical desorption of hydrogen is the rate-limiting step. The small Tafel slope indicates a promising electrocatalyst for HER in practical application. MoS_2/GO composite material has shown superior catalytic behavior compared to that of MoS_2/rGO composite material. The HER catalytic activity of the catalysts is explored using scanning electrochemical microscopy (SECM) using the feedback and redox competition mode in SECM. The activation energy for HER activity was calculated, and the values are in the range of 17–6 kJ/mol. The lower value of activation energy suggested faster HER kinetics.

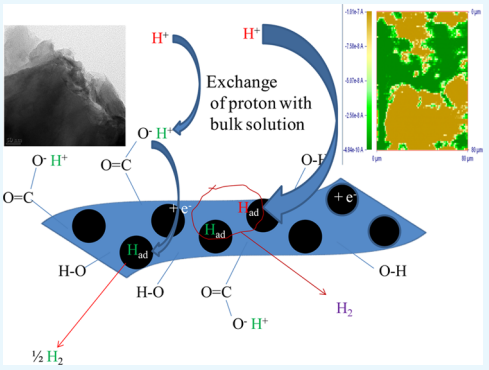

1. INTRODUCTION

The limitation of petroleum fuels and global environmental pollution encourage the researchers to think about an ideal, clean, and efficient alternative source to traditional sources of energy. Hydrogen serves as one of the important alternatives for replacing petroleum fuels for the future. Traditional ways of production of hydrogen involve release of the greenhouse gas CO_2 and a high temperature reaction, and the production of hydrogen through such processes are being phased out.[1] Generation of hydrogen through electrochemical and photoelectrochemical splitting of water is being considered as the favored route for the generation of hydrogen. Such processes require a good electrochemical catalyst which should be cost effective, environment friendly, efficient, and useful in prolonged generation of hydrogen from the splitting of water. As an electrocatalyst, the most important aspect is to decrease the overpotential of splitting water.[2] In acidic solution, Pt group metals are most effective catalysts for the generation of hydrogen but due to the high cost of the Pt group metal elements, large-scale application using these elements is not feasible.[3] Because of the earth's abundant nature, different transition metal alloys, carbides, polymeric carbon nitrides, and transition metal chalcogenides have been investigated for the hydrogen evolution process (HER) catalysis.[4] Molybdenum disulfide has been preferred as a catalyst for HER due to the low cost and high chemical stability.[5] The HER catalytic activity of MoS_2 has been discussed comparing the activity of its 1T and 2H phases. The catalytic activity of 2H phase is mostly through the edges of the catalytic system, and this has been supported using experimental and theoretical studies,[6] and the basal plane was found to have no significant catalytic activity. Therefore, to improve the catalytic activity using 2H-MoS_2, it is essential to have a higher percentage of active edge sites and there has been some report about the catalytic HER reaction using 2H-MoS_2 phase.[7] The activity of the MoS_2 has also been investigated to improve the catalytic activity by making nanophase-based materials. Electrical conductivity of the material has been improved by incorporating Co, Ni, or Fe into nanoscaled MoS_2.[8] Incorporation of Au,[9] activated carbon,[10] carbon paper,[11] or graphite[12] has also been reported to have improved catalytic activity.

There has been tremendous improvement in the electrical conductivity of 1T-MoS_2 compared to 2H-MoS_2, and this has been reflected in the improvement of the HER activity.[13] Even the basal plane of the 1T-MoS_2 is quite electrochemically active for the HER catalytic activity.[13] Therefore, if 1T phase of MoS_2 is formed, there should not be any limitation of its use only through the edge planes. Conductivity of graphene is well understood and accepted for the fabrication of nanophase composite materials of high conductivity.[14] The growth of the

Received: May 26, 2017
Accepted: October 2, 2017
Published: November 2, 2017

DOI: 10.1021/acsomega.7b00678
ACS Omega 2017, 2, 7532–7545

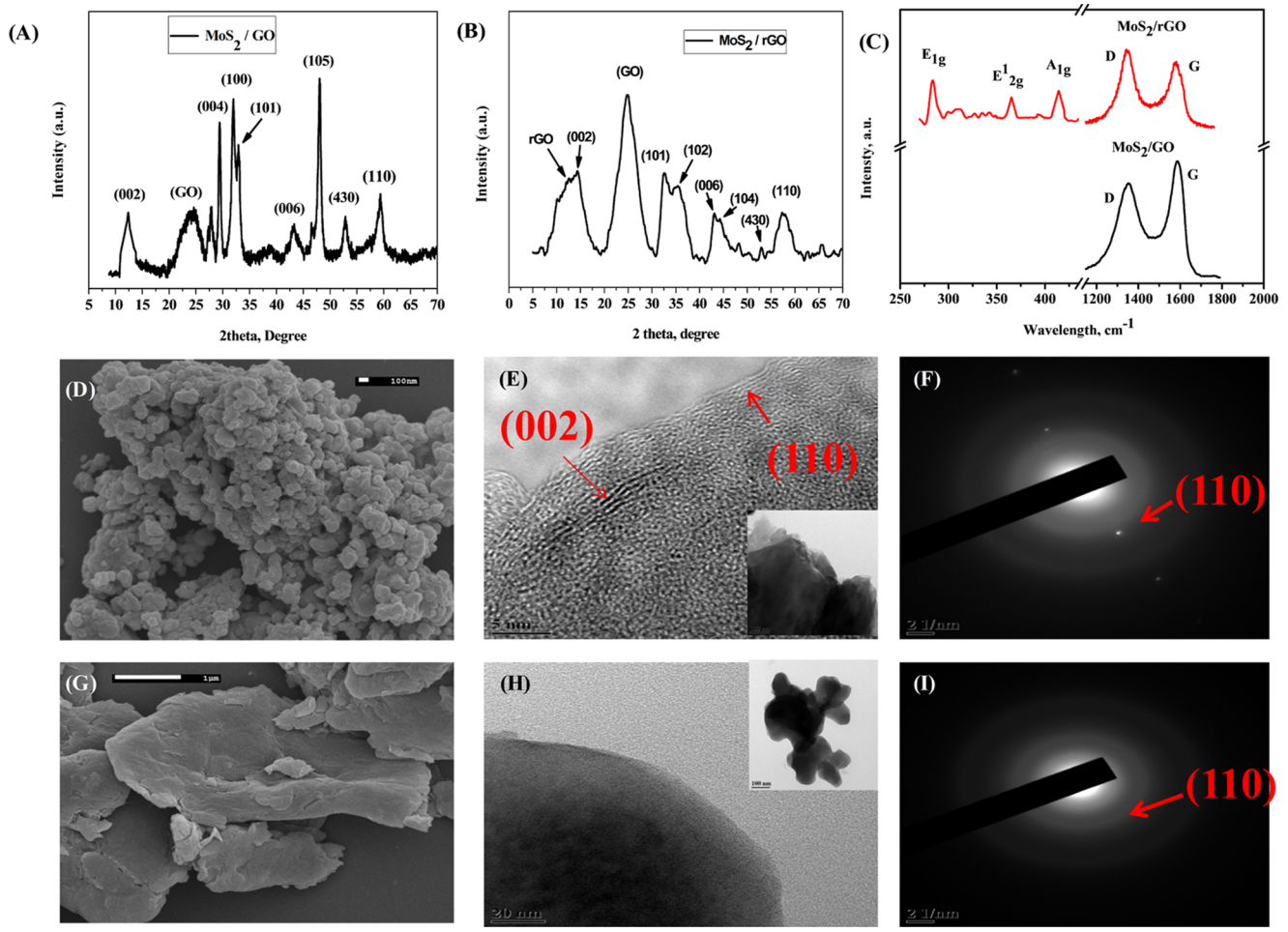

Figure 1. XRD pattern of (A) MoS_2/GO and (B) MoS_2/rGO. Raman spectra of different vibrational modes of (C) MoS_2/GO and MoS_2/rGO. Scanning electron microscopy (SEM) images and transmission electron microscopy (TEM) and selected-area electron diffraction (SAED) patterns of (D–F) pristine MoS_2 and (G–I) MoS_2/rGO. TEM and SAED patterns of MoS_2/GO are shown in the Supporting Information (Figure S2).

catalyst nanophases all over the graphene substrate has further improved the charge-transport property of the catalysts and hence enhanced the HER activity.[4a]

In a previous report, good charge-transfer property between the adjacent layers of MoS_2 and graphene has been reported,[15] which has been the key point in making MoS_2 graphene composites as HER catalysts. Therefore, 1T-MoS_2, with a highly conducting basal plane, when forming composite with graphene, would be the favorable combination for effective transformation into an HER catalyst. Under the present investigation, 1T phase of MoS_2 has been synthesized through the hydrothermal route and the improvement in the catalytic activity of the 1T phase when forming a composite with graphene oxide (GO) and reduced graphene oxide (rGO) has been investigated. Because the entanglement of MoS_2 between the GO and rGO substrate would have some differences, it would be interesting to observe the possible differences in their catalytic activities. The scanning probe electrochemical technique and scanning electrochemical microscopy (SECM) experiments have been employed to map the catalyst substrate using the redox completion mode, and this has reflected the difference in the catalytic behavior between the two composite materials. Probe approach plots at different applied potentials and their transformation from the positive to the negative feed due to the introduction of the redox competition mode between the tip and the substrate has been investigated.

2. RESULTS AND DISCUSSION

2.1. Characterization of the Materials. MoS_2/GO and MoS_2/rGO samples were characterized by X-ray diffraction (XRD) and the diffraction patterns are shown in Figure 1A,B, respectively. Three diffraction peaks 2θ = 12, 43, and 57.5° correspond to (002), (006), and (110) planes of MoS_2, respectively [powder diffraction file (PDF no. 37-1492)], which is due to the metallic 1T structure of MoS_2.[16] The intensity corresponding to the (002) plane of MoS_2/GO is much lower than that of MoS_2/rGO, which suggests that the lower stacking height is along *Z*-axis with more exposure of its active sites. The 1T phase of MoS_2 with a trigonal crystal structure and octahedral orientation is shown to have significant difference in the electronic property compared with the hexagonal 2H phase.[17]

Raman spectroscopy was used for further characterization of phases of MoS_2. The three peaks at 283, 365, and 414 cm^{-1} correspond to the hexagonal vibration modes E_{1g}, $^1E_{2g}$, and A_{1g} of MoS_2, respectively. The in-plane $^1E_{2g}$ and out-of-plane A_{1g} vibrational mode resulted from the opposite vibration of the S atom with respect to the Mo atom, and out-of-plane vibration of only S atom to Mo atom[18] suggests the formation of pure MoS_2 phase. The two bands at 1357 and 1577 cm^{-1} corresponding to the D and G band are clear evidence of graphene sheets in the nanocomposite. As shown in Figure 1C,

DOI: 10.1021/acsomega.7b00678
ACS Omega 2017, 2, 7532–7545

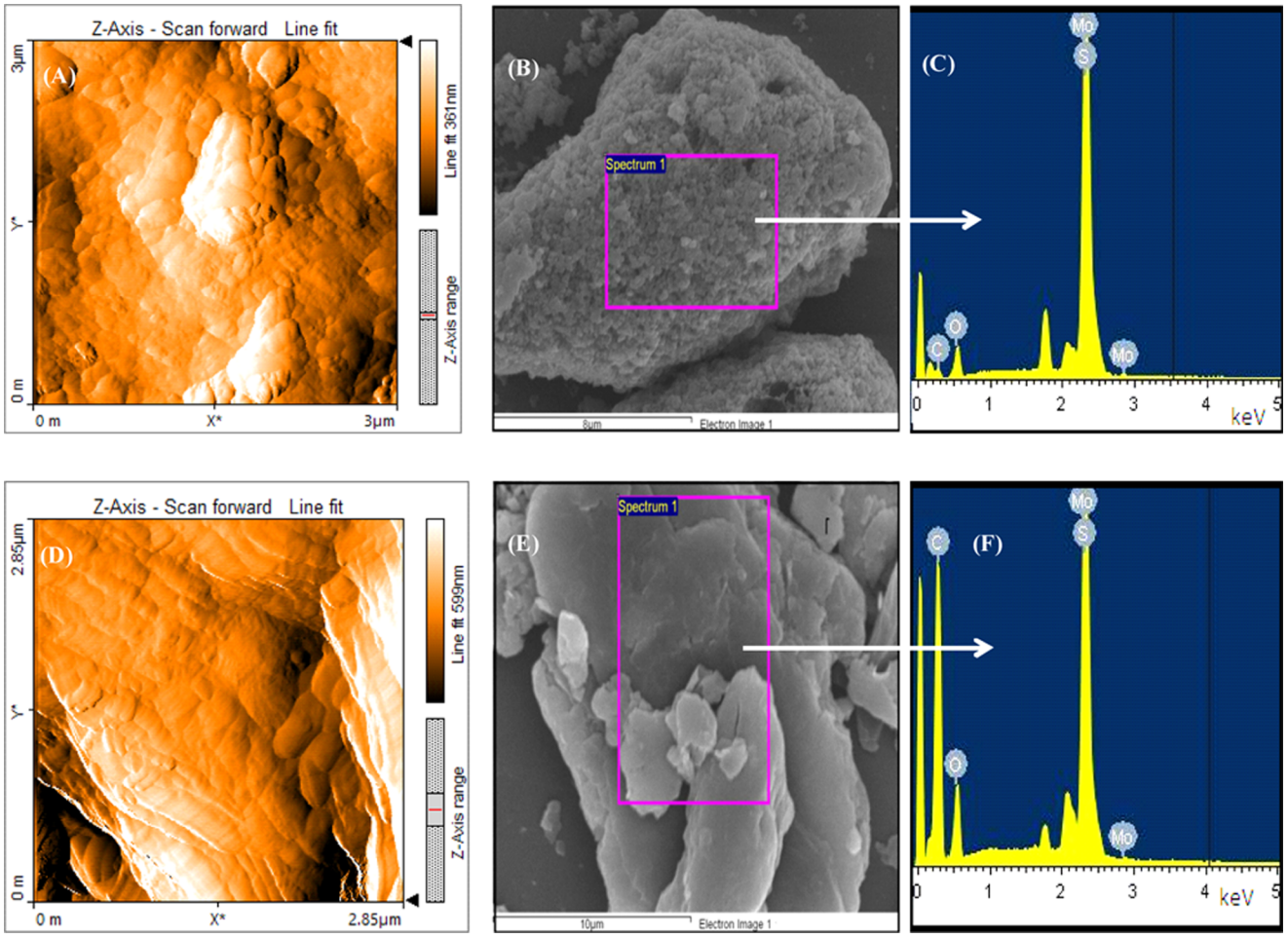

Figure 2. AFM images of MoS_2/GO (A) before the electrochemical test using chronopotentiometry and (D) after the test using chronopotentiometry at 10 mA/cm^2 current density for 4 h. EDS images of (B, C) pristine MoS_2 and (E, F) MoS_2/rGO.

the I_D/I_G ratios of graphene oxide and reduced graphene oxide composite were calculated as 0.92 and 1.07, respectively, which confirmed that GO is reduced to rGO.[19] No significant change in the vibrational mode was observed with the MoS_2 phase during the reduction of GO to rGO. The surface area was measured using the Brunauer–Emmett–Teller method, and the values for MoS_2/GO and MoS_2/rGO were obtained as 65 and 79 m^2/g, respectively.

The morphology and lattice parameters were characterized by SEM and TEM images. Figure 1D,G shows the SEM micrograph of the pristine MoS_2 and the MoS_2/rGO composite materials. The granular nature of the composite for the MoS_2 and sheet-type nature of composite for the MoS_2/rGO composite were observed. TEM images of pristine MoS_2 and MoS_2/rGO are shown in Figure 1E,H, respectively, and the TEM images of MoS_2/GO are shown in Figure S2 of the Supporting Information; both the composite materials have shown a layer type of structure. The selected-area electron diffraction (SAED) of MoS_2 has shown the (002) plane and the (110) plane of MoS_2. The random interconnection between the GO or rGO and MoS_2 network and random stacking of the (002) plane is vulnerable in MoS_2 for the decrease in the catalytic activity.[20] The clear observation of the (002) plane from the SEM and TEM measurements rule out the random stacking of the MoS_2 network. The TEM and SAED of the MoS_2/GO nanocomposite materials shown in Figure S2 of the Supporting Information showed nanostructural characteristics similar to those of the MoS_2/rGO.

The SEM images with EDS results of both the materials are shown in Figure 2. The presence of Mo and S along with C and O is observed. The surface morphology of the catalyst-modified substrate was examined using atomic force microscopy (AFM) measurements using the MoS_2/GO-modified substrate. The morphology has shown a regular granular pattern of the catalyst embedded all over the GO substrate, and the morphology of MoS_2/rGO is shown in Figure S3 of the Supporting Information. The average particle size (diameter) for MoS_2/GO was obtained as 60 nm (the corresponding histograms are shown in Figure S3 in the Supporting Information).

2.2. Electrocatalytic HER Activity. The electrochemical HER activity of the catalyst was investigated in 0.5 M H_2SO_4 solution by depositing catalyst ink on the glassy carbon electrode (GCE) using the three-electrode system, as discussed in the Experimental Procedures. In the polarization curve, the potential is corrected with *iR* drop and with the potential with respect to the reversible hydrogen electrode (RHE). The linear sweep voltammetry (LSV) and cyclic voltammetry (CV) plots for both the catalysts along with the commercially available Pt/C catalyst are shown in Figure 3. The LSV plots of both of the composite materials have shown a sharp increase in the catalytic hydrogen evolution current after the onset potential. The onset potential for the MoS_2/GO is lower by ~0.13 V than that for MoS_2/rGO; however, when compared with the Pt/C catalyst,

DOI: 10.1021/acsomega.7b00678
ACS Omega 2017, 2, 7532–7545

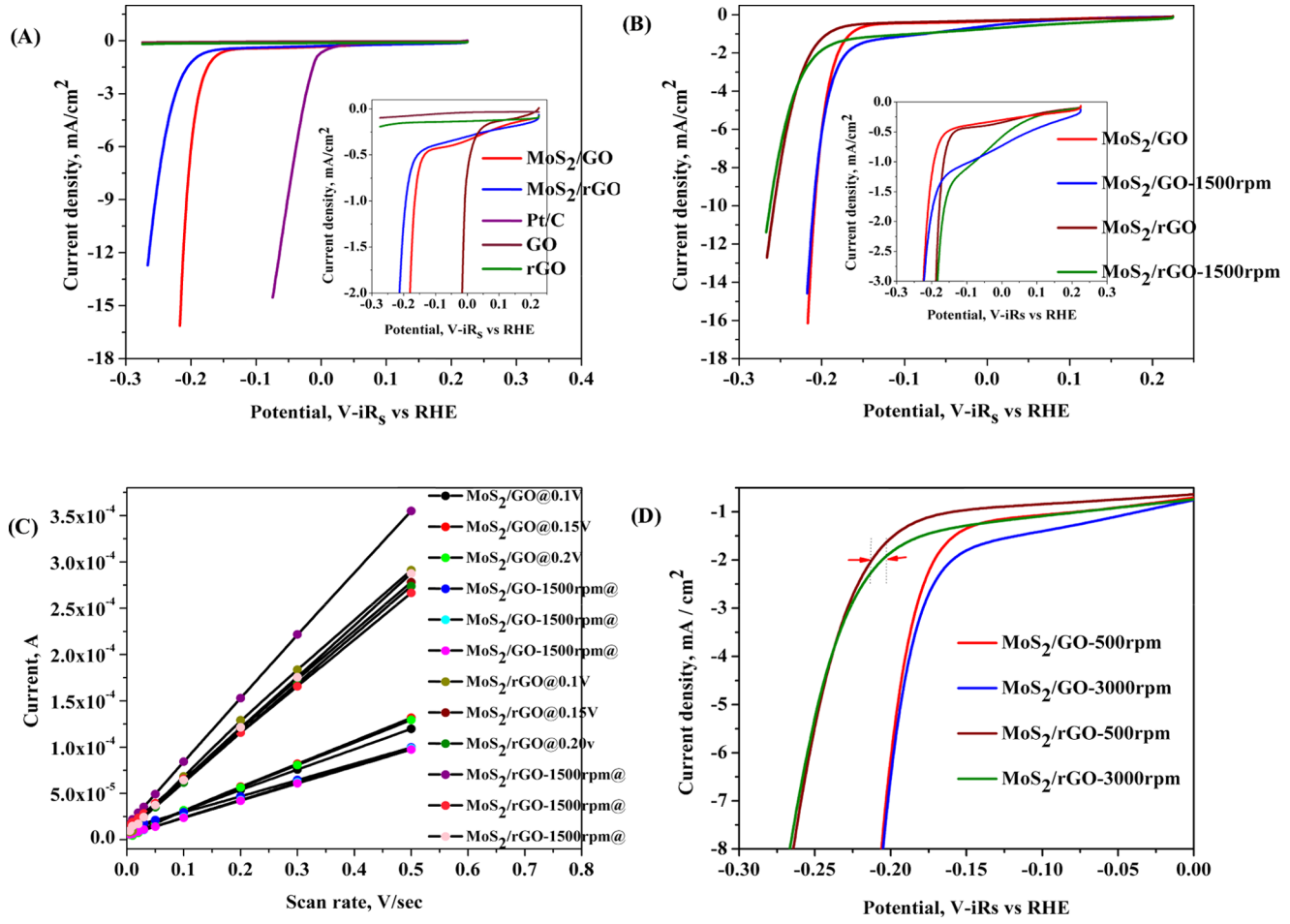

Figure 3. (A) Polarization curve of various catalysts. The magnified image at lower current density is shown as the inset. (B) Polarization curve of catalysts with and without the hydrodynamic effect. The magnified image at lower current density is shown as the inset. (C) Effects of the scan rate on current density. (D) Effect of hydrodynamic conditions on the catalytic activity.

both the materials have shown good electrocatalytic properties and the onset potential is not so inferior to that of the commercially available Pt/C catalyst materials. As seen from Figure 3A, the catalytic activity of the only GO and only rGO-modified electrode has shown no reduction current due to the reduction of proton. Therefore the GO and rGO played only a synergistic role in catalyzing the hydrogen evolution process along with MoS_2. The onset position of the LSV plots was zoomed and shown as the inset of Figure 3A,B; the reduction current in both the composite materials started increasing at 0.2 V and separated from the base line current of the GO and rGO composite-modified substrates. A peak shape was generated at −0.027 V, just before the onset potential for the hydrogen evolution process. This reduction peak is the partial reduction of MoS_2 at the Mo^{4+} center; later, it was oxidized back to its original oxidation state.[21]

The LSV plots were further recorded under hydrodynamic conditions, and corresponding results in comparison with the data under static condition are shown in Figure 3B. At 1500 rpm, the onset potential was improved in both the composite materials compared to that in the static condition. However, the catalytic current at higher applied potential, beyond −0.15 V, remained the same at static and hydrodynamic conditions. Interestingly, the peak current for the peak observed just before the onset potential was increased under hydrodynamic conditions. LSVs were also compared at two different rotation speeds, as shown in Figure 3C, the onset potential of the hydrogen evolution process was improved in both the materials when the rotation speed was increased from 500 to 3000 rpm. The improvement in the catalytic activity at the low-current region due to the hydrodynamic conditions is due to the enhanced mass transfer attained by the hydrodynamic mass flow.

From the LSV measurements, as discussed in the previous section, the MoS_2/GO has shown better catalytic activity for the hydrogen evolution process in terms of the better onset potential and the high catalytic current density. To delineate the better catalytic activity of the MoS_2/GO composite, the electrochemical surface area of the catalyst surface was measured from the double-layer capacitance (C_{dl}) measurements. CV experiments were carried out at different scan rates, as shown in Figure S5 in the Supporting Information, and the current sampled at three potentials 0.1, 0.15, and 0.2 V, where no significant redox process observed, was plotted with respect to the applied scan rates. The results are shown in Figure 3C; from the slope of the linear plot, the double-layer capacitance was determined and tabulated in Table 1. The "C_{dl}" value was calculated from the slope of the current density and scan rate plot.[22]

The C_{dl} values of MoS_2/GO and MoS_2/rGO are obtained as 0.34 and 0.72 mF, respectively. The effect of hydrodynamics on the C_{dl} value shows that the C_{dl} value increases for MoS_2/rGO

DOI: 10.1021/acsomega.7b00678
ACS Omega 2017, 2, 7532−7545

Table 1. Electrochemical Parameters as Obtained from the Cyclic Voltammetry Measurements at Different Scan Rates

name of catalysts	potentials (V)	C_{dl} (F)	$R_f = C_{dl}/60$ μF cm^{-2}
MoS_2/GO	0.20	2.53×10^{-4}	4.21
	0.15	2.55×10^{-4}	4.25
	0.10	2.27×10^{-4}	3.78
MoS_2/GO-1500 rpm	0.20	1.85×10^{-4}	3.08
	0.15	1.85×10^{-4}	3.08
	0.10	1.72×10^{-4}	2.87
MoS_2/rGO	0.20	5.3×10^{-4}	8.83
	0.15	5.31×10^{-4}	8.85
	0.10	5.76×10^{-4}	9.6
MoS_2/rGO-1500 rpm	0.20	5.06×10^{-4}	8.43
	0.15	5.58×10^{-4}	9.3
	0.10	6.81×10^{-4}	11.35

from 0.72 to 0.87 mF; however, the C_{dl} value decreases for MoS_2/GO from 0.34 to 0.27 mF. The roughness factor was calculated from the double-layer capacitance using the following equation

$$R_f = C_{dl}/60 \quad (1)$$

where, the value "60" represents the specific capacitance of a smooth surface in μF cm^{-2}.[23] As seen from Table 1, the R_f value for MoS_2/rGO is higher than that of MoS_2/GO, so it is HER activity should have been higher than that of MoS_2/GO; however, the polarization curve shows that MoS_2/GO has better catalytic activity. This contradicts the above observation. Therefore, the observation of higher catalytic activity in the case of MoS_2/GO compared to that in the case of MoS_2/rGO indicates that the higher catalytic current in the case of MoS_2/GO is not related to the surface area of the materials and has something to do with the inherent characteristics of the HER process over the catalyst's substrate.

The improvement of the onset potential due to the introduction of the hydrodynamic conditions has been mentioned with the discussion of the results in Figure 3. Hydrodynamic conditions were further discussed by determining the kinetic parameters. As shown in Figure 3D, no significant effect of rotation on catalytic activity was observed at the higher overpotential range but at lower overpotential the catalytic current is modified significantly. At 2 mA/cm^2 current density, the applied potential was improved by 13.1 mV in the case of MoS_2/GO and improved by 7.4 mV in the case of MoS_2/rGO when the rotation speed was increased from 500 to 3000 rpm. Detailed kinetic information about the contribution from the mass flow and the charge-transfer kinetics was investigated by introducing the Koutechy–Levich analysis[24] using the equations as follows

$$\frac{1}{i} = \frac{1}{i_k} + \frac{1}{i_l}$$

$$\frac{1}{i} = \frac{1}{i_k} + \frac{1}{B\omega^{1/2}} \quad (2)$$

where $i_k = nFAkC_0$ and $B = 0.2nFC_0D^{2/3}\nu^{-1/6}$ and, i, i_k, and i_l are the measured current, kinetic current, and limiting current, respectively. ω is the rotation rate of the electrode in rpm. k is electron-transfer rate constant; n is the number of electron transfers; F = 96 500 C/mol; A is the surface area of RDE in cm^2; C_0 is the concentration of H^+ in bulk solution in mol/cm^3; D is the diffusion coefficient of proton in 0.5 M H_2SO_4, and its value corresponds to 9.3×10^{-5} cm^2 s^{-1}; and ν is the kinematic viscosity of 0.5 M H_2SO_4, and its value is 0.01 cm^2 s^{-1}.[25] Currents were sampled at different applied potentials of the LSV plot (Figure 4) during the Koutechy–Levich analysis, and the corresponding kinetic parameters for both the composite materials are shown in Table 2. At a lower applied potential below the onset potential, the number of electrons transferred was obtained as close to one, at a higher applied potential (at −0.21 V) the number of electrons transferred increased significantly. Such an unreasonably high value of the number of electrons transferred for the HER process is accounted for by the enhanced mass flow which resulted in the increased surface concentration of the H^+ compared to its bulk concentration. The electron-transfer rate constant of the HER process in MoS_2/rGO catalyst was marginally higher than that in the MoS_2/GO catalytic system (Table 3).

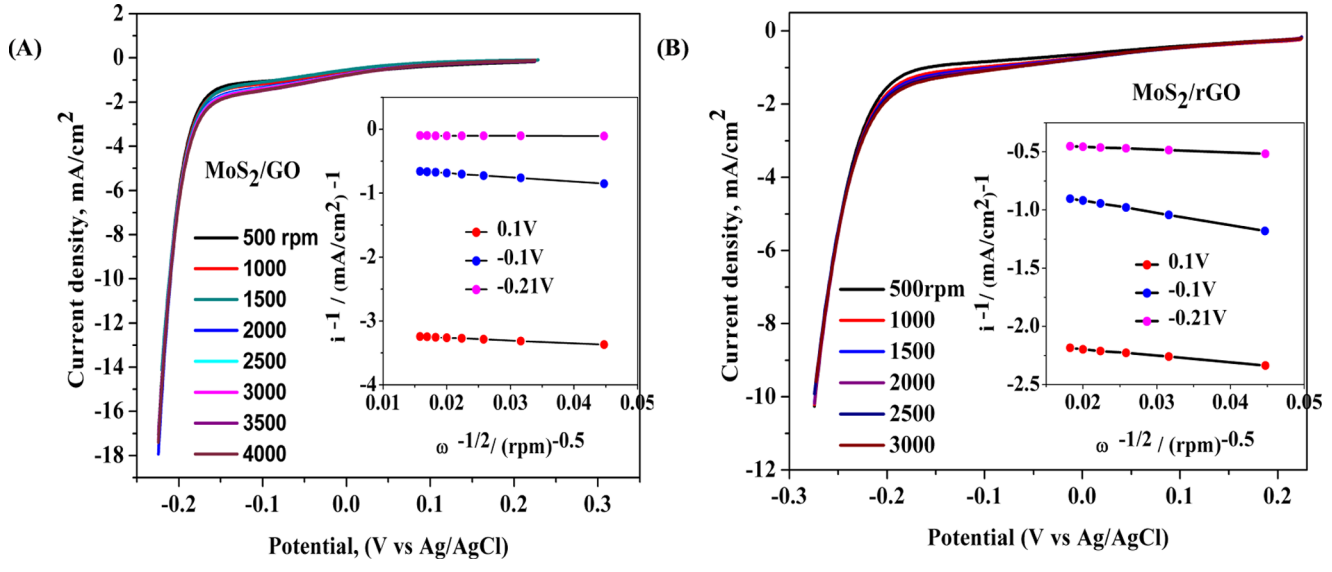

Figure 4. Koutechy–Levich plot of (A) MoS_2/GO and (B) MoS_2/rGO.

DOI: 10.1021/acsomega.7b00678
ACS Omega 2017, 2, 7532–7545

Table 2. Analysis Results from the Hydrodynamic Voltammetric Measurements Using the Koutechy–Levich Analysis[a]

name of catalyst	potential (V)	slope	intercept	1/intercept, i_k in mA/cm^2	n	k, cm/s
MoS_2/GO	0.1	−4.413	−3.5726	−0.2799	1.15	5.06×10^{-3}
MoS_2/GO	−0.1	−6.66	−0.552	−1.811	0.76	49.45×10^{-3}
MoS_2/GO	−0.21	−0.181	−0.0969	−10.3199	27.91	7.66×10^{-3}
MoS_2/rGO	0.1	−5.72	−2.0819	−0.48	0.88	11.26×10^{-3}
MoS_2/rGO	−0.1	−10.585	−0.70643	−1.4155	0.47	61.41×10^{-3}
MoS_2/rGO	−0.21	−2.431	−0.4076	−2.45339	2.08	24.44×10^{-3}

[a]The final values of n and k are rounded off to two decimal places.

Table 3. Activation Energies Obtained on Two Catalytic Systems at Different Applied Potentials

$\ln i = \ln i_o - E_a^{app}/RT$		
overpotential, V	E_a^{app} of MoS_2/GO, kJ/mol	E_a^{app} of MoS_2/rGO, kJ/mol
0.10	17	20
0.15	14	19
0.21	6	10

Temperature-dependent electrochemical measurements were carried out in a custom-made cell, in which water can be filled in the outer jacket for temperature control; corresponding results for the MoS_2/GO materials are shown in Figure 5A. The reference electrode was corrected for temperature using the following equation.[26]

$$E^\circ\,(\mathrm{V})_{Ag/AgCl} = 0.23695 - 4.8564 \times 10^{-4}\, t - 3.4205 \times 10^{-6}\, t^2 \quad (3)$$

LSVs at different temperatures varying from 5 to 70 °C were recorded. The Ag/AgCl reference electrode was calibrated for different temperatures using the above equation. Figure 5A shows the temperature-dependent LSV for the MoS_2/GO catalyst, and the results indicated the improvement of the onset potential for the HER process with rise in temperature.

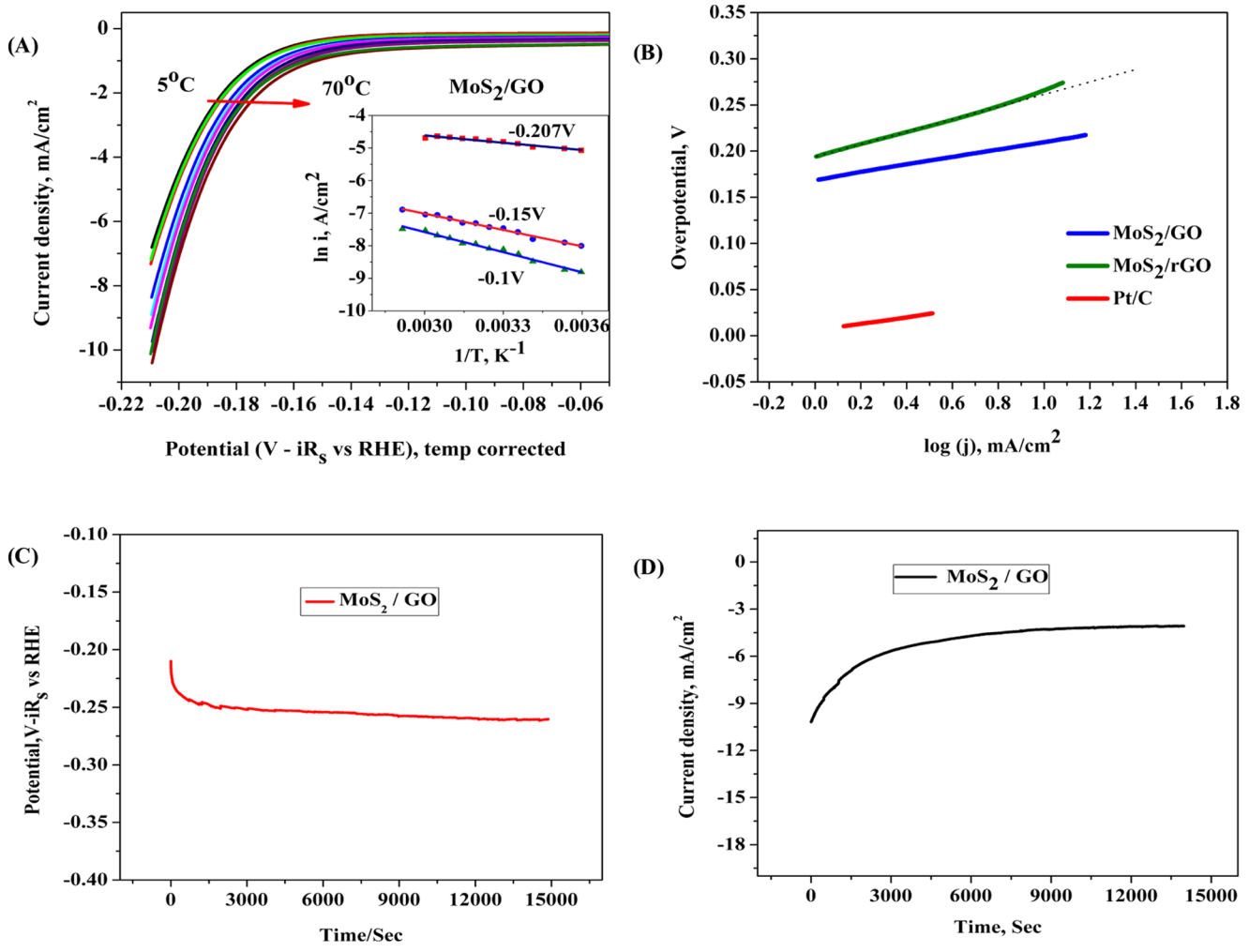

Figure 5. (A) Temperature-dependent polarization curve for MoS_2/GO. Arrhenius plot is shown as inset; (B) Tafel plot of the two-catalyst system in comparison with that of the standard Pt/C catalyst; (C) stability test using chronopotentiometry; and (D) stability test using chronoamperometry of MoS_2/GO catalyst.

DOI: 10.1021/acsomega.7b00678
ACS Omega 2017, 2, 7532−7545

Corresponding results for the MoS_2/rGO composite materials are shown in Figure S6 of the Supporting Information. To evaluate and extract the activity of the electrocatalysts, the apparent activation energy for hydrogen evolution (E_a^{app}) is estimated using the following equation.[27]

$$\frac{\partial \ln i}{\partial\left(\frac{1}{T}\right)} = -\frac{E_a^{app}}{R} \quad (4)$$

where E_a^{app} is evaluated at different applied potentials, i is the current density at a given applied potential, T is the absolute temperature, and R is the universal gas constant. After recording the LSVs at different temperatures, the observed currents were sampled at three different applied potentials and $\ln i$ versus $1/T$ plots at three different applied potentials are shown in the inset of Figure 5A. It was observed that the slopes of the plots were decreased with the application of more cathodic potential, indicating potential-dependent apparent activation energy for the overall process. The apparent activation energy for MoS_2/GO composite material is relatively lower than that of the MoS_2/rGO at all applied potentials. Because the activation energy is calculated from the change in the overall current with the change in temperature of the process (mass transfer and charge transfer), the effect of the change in temperature will be reflected in the activation energy calculation. Therefore, the relatively low activation energy in MoS_2/GO material might be due to the enhanced mass transfer compared to that of MoS_2/rGO.

Tafel treatment was applied to the LSV plot, and the linear portion of the Tafel plot in Figure 5B was fitted using the Tafel equation, $\eta = a + b \log j$, where j is the current density and b is the Tafel slope. The Tafel slopes for the corresponding catalyst materials MoS_2/GO and MoS_2/rGO are obtained as ≈ 40.6 and ≈ 71.8 mV/decade, respectively. The overpotential is iR_s-corrected and on the scale of the RHE value, as shown in eq 9. The Tafel slope is used to elucidate the mechanisms involved in the HER process. There are three possible reaction steps in acidic aqueous medium for the HER process.[28] First, the discharge step (Volmer reaction)

$$H_3O^+ + e^- \rightarrow H_{ads} + H_2O \quad (5)$$

where the Tafel slope, $b = 2.3RT/\alpha$, $F \approx 120$ mV/decade, R is the universal gas constant, T is the absolute temperature, $\alpha = 0.5$ is the symmetry coefficient, and F is the Faraday constant. The second step is the combination step (Tafel reaction)

$$H_{ads} + H_{ads} \rightarrow H_2 \quad (6)$$

$$b = 2.3RT/2F \approx 30\text{mV/decade}$$

The third step is the electrochemical desorption step (Heyrovsky reaction)

$$H_{ads} + H_3O^+ + e^- \rightarrow H_2 + H_2O \quad (7)$$

$$b = 2.3RT/(1 + \alpha)F \approx 40 \text{ mV/decade}$$

The Tafel slope is an inherent property of the catalyst that is determined by the rate-limiting step of the HER process. Generally, the fast-discharging step 5 is followed by either the combination step 6 or electrochemical desorption step 7. If the fast-discharging step 5 is followed by the rate-limiting combination step 6, the Tafel slope will be ~30 mV/decade; in this case, the overall mechanism of the process would be the Volmer–Tafel mechanism. If the fast-discharging step 5 is followed by slow electrochemical desorption step 7, the Tafel slope will be ~40 mV/decade and in that case, the HER mechanism would be the Volmer–Heyrovsky mechanism. When the electrochemical discharging step is the rate-limiting step, the Tafel plot will be ~120 mV/decade and the mechanism will be through the Volmer step as the rate-determining step.[28,29]

The observed Tafel slope of ~40.6 mV/decade in the present case, as seen from Figure 5B for the MoS_2/GO hybrid catalyst, suggests that the electrochemical desorption step would be the rate-limiting step of the present system. In the case of the MoS_2/rGO hybrid catalyst, the Tafel slope was observed as 71.8 mV/decade. The mechanism of the hydrogen evolution process over the MoS_2 catalytic system is such that the discharge step predominates over the Mo center and S and graphene centers are responsible for the adsorption and further recombination process for liberating hydrogen gas out of the catalytic system. Mo centers are similar in both the catalytic systems, and the major difference would arise due to the difference in the GO and rGO in the catalysts. The significantly higher Tafel slope in the case of the MoS_2/rGO hybrid catalyst system is indicative of mixed mechanism operating across the catalyst substrate. A part of the catalyst substrate having Mo centers would have a fast discharge process, whereas the rest of the surfaces result in the slow discharge kinetics making the overall Tafel slope high.[7c,30] In the case of the MoS_2/GO hybrid catalyst system, there are plenty of exchangeable H^+ ions all over the matrix; because of such exchange of H^+ ions between the solution and the −COOH and −OH groups present over the catalytic substrate, the discharge step would be quite fast.[31] The electrochemical reduction of H^+ has been consolidated and presented in Scheme 1.

Scheme 1. Proposed Mechanism of the HER Process over the MoS_2/GO Substrate

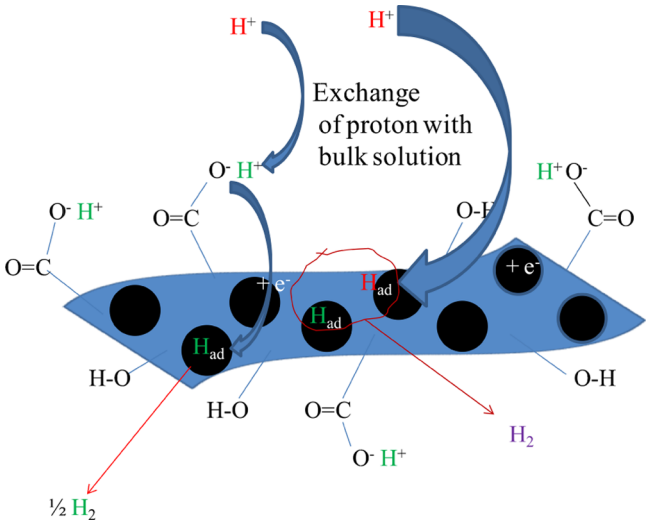

Furthermore, the stability of the catalyst was tested by the chronopotentiometry and chronoamperometry method. Chronopotentiometry experiments were carried out at the current density of 10 mA/cm^2 for 4 h. As seen from the results in Figure 5C, the MoS_2/GO catalyst is quite stable at the experimental time period and the applied potential remained below −0.25 V for the chosen current density. Chronoamperometric experiments were carried out at an applied potential of

DOI: 10.1021/acsomega.7b00678
ACS Omega 2017, 2, 7532–7545

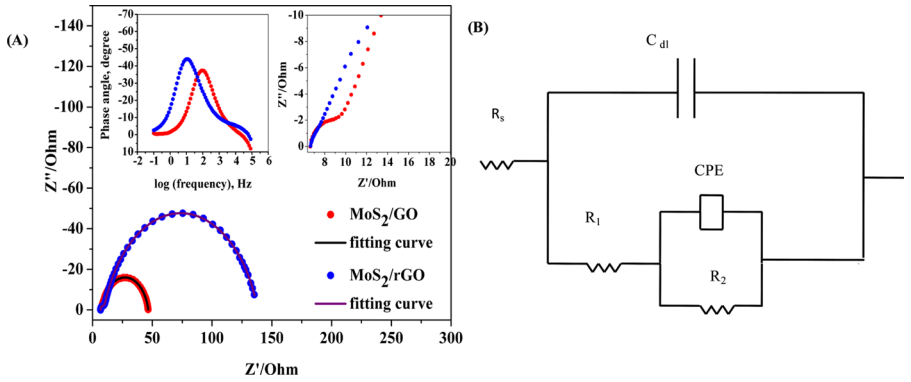

Figure 6. (A) Nyquist plot of MoS_2/GO and MoS_2/rGO. Inset: zoomed portion of the Nyquist plot at the high-frequency region and the corresponding Bode plot at the entire frequency range. (B) The equivalent circuit used for fitting the impedance results.

−0.20 V, and it was observed that after an initial drop in current, it remained stable for the experimental time period of 4 h. Even though the 1T phase of MoS_2 is said to be in the metastable phase, composites of 1T-MoS_2 have been stable even after long-term testing.[13a] GO and rGO might have an important role in stabilizing the 1T-MoS_2 phase on prolonged HER catalysis.

The catalyst-modified electrode was examined using AFM measurements after the stability test, that is, the chronoamperometric experiments, for 4 h. As seen from Figure 2D, the general morphology of the materials remained similar to that of what there was before the electrochemical test. From the histogram and AFM micrograph (Figures S3 and S4 of the Supporting Information), the average particle size was decreased from 60 to 40 nm after the electrochemical test. The layered structure of composite materials well appears after the electrochemical test. Because of the energetic changes during the electrochemical test, the materials might have relaxed, which has resulted in the minor modification in the morphology of the composite materials. A similar observation was reported previously on the Mo oxide materials, where in prolonged electrochemical cycles, the size of the Mo oxide nanoparticles was decreased; such decrease in the size of the nanoparticles and the morphological change were described due to the redox activities at the catalytic center in prolonged electrochemical cycles.[32]

2.3. Electrochemical Impedance Measurements. The charge-transfer efficiency of the electrocatalyst was investigated by electrochemical impedance spectroscopy using the CH Instrument by applying an alternating current voltage of 10 mV amplitude in a frequency range of 100 000−0.1 Hz. Corresponding results in the form of the Nyquist plot and the circuit used for fitting the Nyquist plot are shown in Figure 6. The zoomed portion of the high-frequency region of the Nyquist plot is shown as the inset of Figure 6. The Nyquist plot was characterized with two semicircular regions, one at a high frequency and the other at the low frequency. The Nyquist plots were fitted with the equivalent circuit model, as shown in Figure 6. Here, R_s represents solution resistance, R_1 is the charge-transfer resistance, and R_2 is the resistance incorporated to account for the second semicircle.[30a,33] The total resistance for the Faradaic process of HER is the sum of R_1 and R_2. From Figure 6A, the R_1 value for MoS_2/GO is 6 Ω, which is lower than that of MoS_2/rGO, 8 Ω. The value of R_2 in the case of MoS_2/GO (32 Ω) is significantly lower than that in the case of MoS_2/rGO (120 Ω). Corresponding to the mechanism of the overall process, as discussed in the Tafel analysis, the resistance R_1 corresponds to the Volmer step and the resistance at the low-frequency region R_2 corresponds to the desorptive charge-transfer process, the Heyrovsky step. A smaller value of R_1 in both the materials suggests a better charge-transfer possibility. The semicircular loop at the low-frequency region corresponds to the desorptive charge-transfer process, and this process has a dominant role in the overall HER kinetics. A considerably low value of this desorptive resistance in the case of MoS_2/GO composite material compared to that in the case of MoS_2/rGO material has indicated that the difference between the HER activity between these two materials is due to the difference in this adsorption resistance.[34] The Bode phase plot is shown as the inset of Figure 6A, and it has been observed that at 0.215 V of overpotential, the phase angle maxima value is 37° for GO composite, which is smaller than that of the rGO composite at 44°. The lower phase angle maxima suggests an improved Faradaic process in the case of GO composite materials compared to that in the case of rGO composite materials.[35] Similar to the CV measurements, the roughness factor (R_f) was determined from the capacitance value obtained from the impedance measurements and the values are obtained as 4.33 and 11.5 for MoS_2/GO and MoS_2/rGO composite materials, respectively.

Additionally, the phase angle maxima for the relaxation process associated with surface intermediates falls in the range of 10−100 Hz. The relaxation frequencies for MoS_2/GO and MoS_2/rGO composites are 100 and 20.89 Hz, respectively. This relaxation process is due to the nonhomogeneous charge transfer by the surface species. Above the onset potential of hydrogen evolution, the relaxation due to nonhomogeneous charge distribution dominates, with a minor contribution from the double-layer capacitance and charge-transfer components, as shown in Figure 6A. However, the phase angle maxima for the GO composite being at a higher frequency than that of the rGO composite suggests that there is significant masking due to the double-layer capacitance on the HER activity in the case of the GO composite. This double-layer masking effect should limit the performance of MoS_2/GO composite but the performance of MoS_2/GO is better than that of rGO, as shown in Figure 6A. This anomalous property can be explained through the functionalized GO with hydroxyl and carboxylic acid groups that might increase the double-layer masking and at the same time increase the mass flow of protons through the exchange mechanism from the acidic solution, as shown in Scheme 1.

DOI: 10.1021/acsomega.7b00678
ACS Omega 2017, 2, 7532−7545

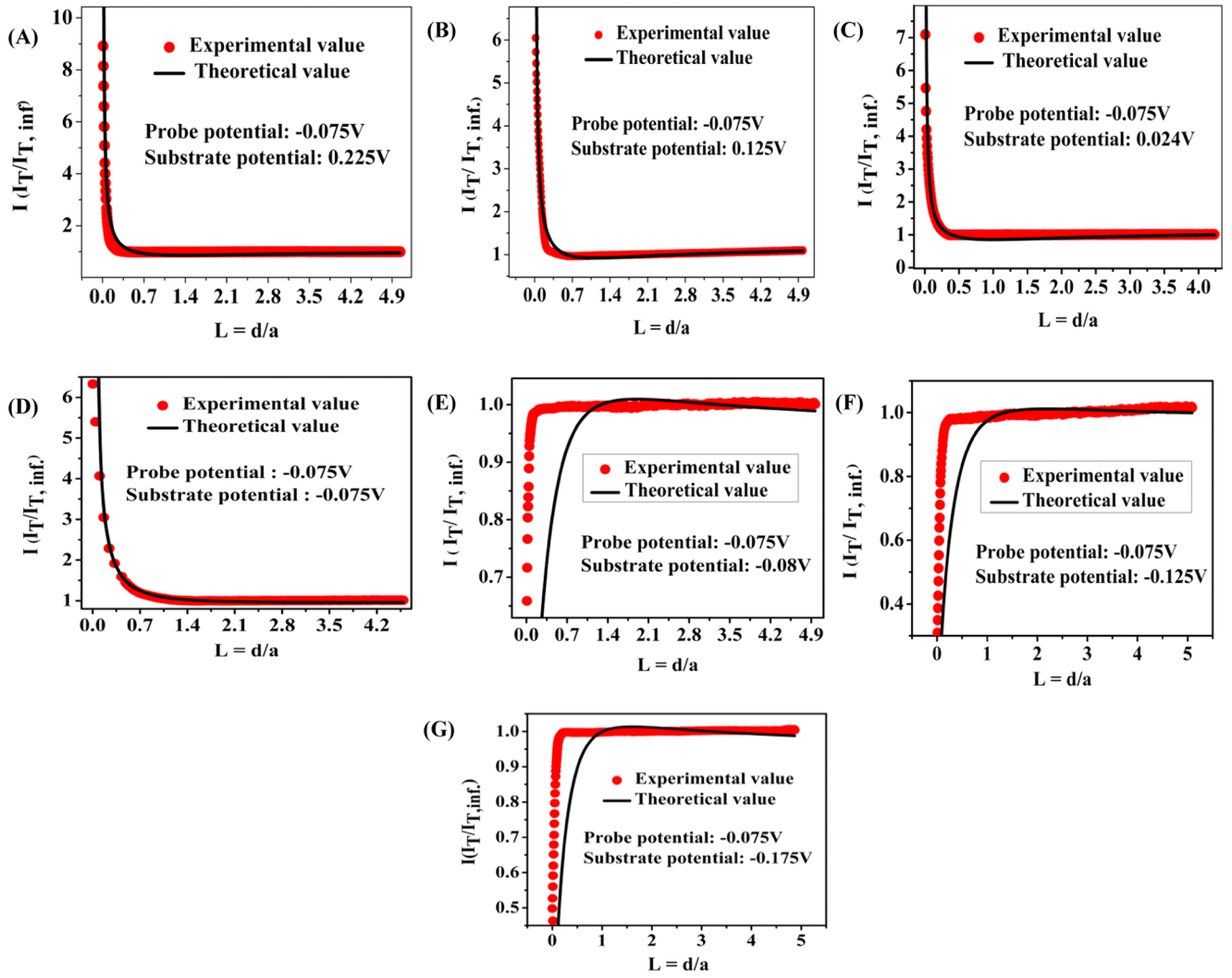

Figure 7. Probe approach curve (PAC) for the MoS_2/GO catalyst at different substrate potentials (A) 0.225 V, (B) 0.125 V, (C) 0.024 V, (D) −0.075 V, (E) −0.08 V, (F) −0.125 V, and (G) −0.175 V, keeping a constant probe potential at −0.075 V.

2.4. Scanning Electrochemical Microscopy Measurements. Scanning electrochemical microscopy (SECM) was employed to characterize the charge-transport processes and to obtain the local electrochemical activity of the substrates. A Pt ultramicro electrode (UME) of diameter 10 μm was used as the working electrode (probe or tip electrode), Pt wire was used as the counter electrode, the saturated Ag/AgCl electrode as the reference electrode, and the glassy carbon electrode (GCE) modified by the catalyst was used as the substrate electrode. The approach of probe to the surface of the catalyst was performed by the probe approach curve (PAC) technique, in which a constant potential of −0.075 V versus RHE was applied to the probe and different potentials in the range from 0.225 to −0.175 V were applied to the substrate. Electrochemical signals were measured by measuring the current at the UME tip as a function of the precise tip position over the substrate at the approach distance, and the SECM imaging was obtained. The steady-state probe current is given by[36]

$$I_d = 4nFCDa \quad (8)$$

where I_d is the diffusion-limited current, n is the number of electrons transferred at the electrode tip, F is Faraday's constant, C is the concentration of H^+ ions in solution, D is the diffusion coefficient, and a is the radius of the UME disk. In bulk solution, H^+ ions got reduced at the UME tip and produced a steady-state current limited by hemispherical diffusion. As the tip approached the substrate, the hydrogen atom formed after reduction of the H^+ ions at the tip oxidized at the substrate, when the potential applied at the substrate is more positive than the tip potential and a positive feedback response was observed;[36b] although the catalyst substrate was not meant for the oxidation of hydrogen to proton, at an applied positive potential it should oxidize hydrogen to proton. Feedback responses at different substrate potentials are shown in Figure 7, where the normalized current, the tip current during approach (i_T), is divided by the steady-state tip current when the tip was in the bulk solution (i_{Tinf}), which is plotted with respect to the normalized distance L (d/a), where d is the tip-to-substrate distance and "a" is the radius of the tip electrode. Positive feedback response was obtained when the substrate potential was more positive or equal to the tip potential, and negative feedback responses were obtained when substrate potentials were more negative than the tip potential. This is due to the enhanced mass flow of H^+ to the tip at a relatively positive applied potential at the substrate. The negative feedback response was due to the redox competition

DOI: 10.1021/acsomega.7b00678
ACS Omega 2017, 2, 7532−7545

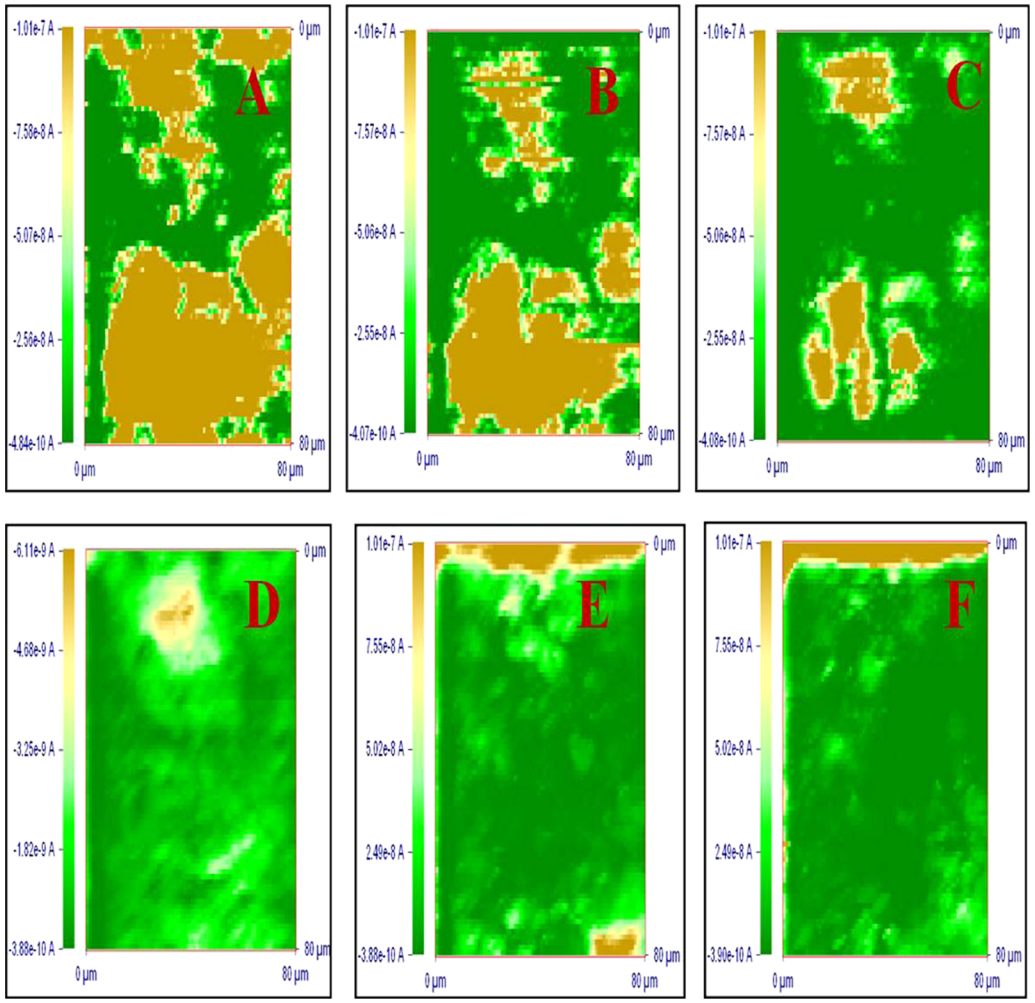

Figure 8. Scanning electrochemical microscopy (SECM) images of MoS_2/GO catalyst at different substrate potentials (A) 0.225 V, (B) 0.125 V, (C) 0.025 V, (D) −0.075 V, (E) −0.125 V, and (F) −0.175 V.

between the tip and the substrate. When the potential at the substrate was same or more negative, reduction of H^+ ions became prominent at the substrate; hence, negative feedback responses were obtained. Therefore, at the same applied potential to the tip and the substrate, the substrate could impose a negative feedback response to the tip due to the introduction of the redox competition mode into the system. This is essentially due to the higher surface area of the substrate and also the good catalytic activity of the substrate. The feedback responses were fitted with standard models, as seen from Figure 7, where most of the positive feedback responses could be fitted reasonably well; however, the negative feedback responses could not be fitted due to the redox completion mode operating between the tip and the substrate.

After the probe approached the substrate, the catalyst-modified substrate was scanned for the electrochemical imaging of the substrate by SECM using the steady-state current response from the tip.[36a] The SECM scanning was carried out in the constant height mode, where the distance between the probe and the substrate was kept constant at the approach distance of 1.1 μm and the probe was scanned in the $X-Y$ plane. The SECM scans for the MoS_2/GO materials are shown in Figure 8. It was observed that at the relatively positive substrate potential, the overall probe current was high all over the substrate; there were some high-current regions spread across the whole substrate. With a shift in the applied potential toward more negative direction, the spread of the high-current regions were decreased and only a few high-current inlands were observed at the substrate potential of 0.025 V. At −0.075 V, the transition potential between the positive and the negative feedback response, the entire substrate was covered with low current response. At further negative applied potential to the substrate, the probe recorded very low negative currents across the substrate with some inlands of positive current, as seen in Figure 8E. The positive current response from the probe was further increased at even more negative applied potential to the substrate (cf. Figure 8F). The probe approach plots and the SECM scans for the MoS_2/rGO materials are shown in Figure S7 of the Supporting Information. A nearly similar observation as that for the MoS_2/GO hybrid material was observed in the probe approach plot and SECM scan at different potentials. When the corresponding figures of Figure 8E,F were compared with Figure S7E,F, it was observed that the positive current response from the tip was higher in the case of MoS_2/GO than in the case of MoS_2/rGO. Thus, the more prominent positive current response at the substrate potentials of −0.125 and −0.175 V in the case of MoS_2/GO hybrid materials compared to that in the case of the MoS_2/rGO hybrid material, indicates a better catalytic hydrogen evolution process over the MoS_2/GO. SECM was used previously for the investigation of HER

DOI: 10.1021/acsomega.7b00678
ACS Omega 2017, 2, 7532−7545

processes and it was reported that the strained S vacancy of MoS_2 has much higher HER activity than an unstrained one.[37] The present result on SECM revealed that both the composite materials have imposed the oxidation reaction at the Pt tip at an applied substrate potential of −0.075 V; however, the oxidation process at the tip due to the redox competition process is induced predominantly by the MoS_2/GO composite materials than the MoS_2/rGO composite materials. Both the materials have shown good catalytic activity for the HER process, with relatively higher activity for MoS_2/GO composite material, which has been revealed from the LSV measurements and supported by the impedance and hydrodynamic measurements. Previous investigation on SECM with surface interrogation has revealed the Mo−H bond formation during the HER catalysis process using MoS_2 catalyst.[38] This Mo−H bond formation might be facilitated due to the presence of adjacent exchangeable protons in MoS_2/GO composite materials.

The difference in the work function between graphene and MoS_2 has been favorable for the electron to flow from MoS_2 toward the graphene sheet; good coupling between the MoS_2 and the graphene sheet would always make this flow of electron fast for an efficient HER process.[15]

The present observation of the enhanced HER process in the case MoS_2/GO composite materials is explained from the direction of the electron flow from MoS_2 to the graphene sheets. The electron would transfer from the electrode to MoS_2, which will further be transferred to the graphene sheet, from which the electron will be transferred to H^+ ions, and the charge-transfer reaction will take place for the HER catalytic reaction. Because there are exchangeable protons already present in the graphene sheet of GO, the overall charge-transfer process would always be favored in the case of MoS_2/GO composite materials compared with MoS_2/rGO composite materials.[39]

3. CONCLUSIONS

The composites of GO ad rGO with the MoS_2 have been synthesized. Material characterization has revealed the 1T phase of MoS_2. Both the composite materials have shown very good catalytic activity for HER process and their catalytic activities are not so inferior to the commercially available Pt/C catalyst. Electrochemical investigations with Tafel analysis have indicated the Volmer−Heyrovsky mechanism for the HER process in the MoS_2/GO catalytic system. LSV experiments were carried out in the hydrodynamic mode and the results are shown to have a marginally higher electron-transfer rate constant for MoS_2/rGO composite materials, where the current density and the onset potential for the HER process was comparatively favorable in the case of MoS_2/GO. Such anomaly in the observation has indicated the enhanced mass transfer process for MoS_2/GO; such enhanced mass transfer has been ascertained from the exchange of proton at the functional group over the GO matrix and the bulk acidic solution. Electrochemical impedance measurements have shown to have high desorptive charge-transfer resistance for MoS_2/rGO composite material responsible for the comparatively low HER. SECM experiments were carried out using the catalyst-modified substrate, and the probe approach plot has shown the transformation of the composite-modified electrode as the substrate from oxidation of proton to the efficient HER catalyst with the modulation of the applied potential. The SECM substrate scan has shown the enhanced oxidation current from the tip electrode at a cathodic applied potential to the MoS_2/GO composite-modified substrate compared to that in the MoS_2/rGO composite-modified substrate.

4. EXPERIMENTAL PROCEDURES

4.1. Preparation of MoS_2 Nanoparticle. MoS_2 was synthesized by the hydrothermal method. Ammonium molybdate ($(NH_4)_6Mo_7O_{24}\cdot 4H_2O$, 0.44 gm) was dissolved in 5 mL of deionized water and then hydrazine hydrate ($N_2H_4\cdot H_2O$, 86%, 4 mL) as the reducing agent was added dropwise under stirring condition. The reaction mixture was stirred for 0.5 h, and then sodium sulfide (Na_2S, 1.32 g) dissolved in 5 mL of deionized water was added into it; then, the mixture was left for 10 min for incubation; 5 mL of 2 M HCl was added dropwise to that mixture. Then, the reaction mixture was left for 10 min again for incubation. Thereafter, the reaction mixture was transferred into a 50 mL Teflon-lined stainless steel autoclave and heated at 180 °C for 24 h. After 24 h, the autoclave was allowed to cool at room temperature and then black product was washed with distilled water several times and then with ethanol. The product, as obtained, was dried at 60 °C for 12 h in the vacuum oven. The mole ratio of the reactants was kept at $Mo/N_2H_4/Na_2S$ of 1:357:48 during the synthesis process.

4.2. Synthesis of Graphene Oxide. Graphene oxide was synthesized using the modified Hummer's method.[40] Concentrated H_2SO_4 (300 mL) and H_3PO_4 (40 mL) were taken in a round-bottomed (RB) flask of 1 L capacity. The RB flask was kept in an ice bath at 0−5 °C. The whole setup was kept in a magnetic stirrer; then, graphite (2 g) powder was added into the RB flask slowly and the mixture was kept for stirring for 2 h. Then, $KMnO_4$ (12 g) was added slowly to this mixture under stirring condition; this reaction mixture was stirred for 3 days at room temperature. Thereafter, the reaction mixture was kept in an ice bath; H_2O_2 (20 mL) was added slowly to terminate the reaction, followed by washing with HCl (10%) and then distilled water several times to achieve the neutral pH. The graphene oxide thus obtained was dried in a vacuum oven and used for further experiments. Graphene oxide was reduced by treating GO suspended aqueous solution using hydrazine monohydrate by stirring for 1 h, and then the solution mixture was kept under hydrothermal conditions at 180 °C for 12 h. The rGO thus obtained was washed and dried for further use.

4.3. Procedure of Electrochemical Studies and Instrumentation. MoS_2 and GO or rGO were mixed in mortar (in 1:4 ratios). Then, 1 mg of the sample mixture was suspended in ethanol and water solution (in a 1:1 ratio) and kept in stirring conditions for 24 h. The suspension was sonicated for 1 h, and then 100 μL of nafion (5 wt %) was added and again sonicated for 30 min. After sonication, a homogeneous mixture was formed and then 5 μL of catalyst ink was drop-casted onto the glassy carbon (GC) electrode, which then dried under an IR lamp. Electrochemical measurement for the hydrogen evolution catalysis process was carried out using the CH Instrument model 920D. Electrochemical studies were performed in 0.5 M H_2SO_4 solution using a typical three-electrode setup using the catalyst-modified electrode as the working electrode, Pt wire as the counter electrode and Ag/AgCl electrode as the reference electrode. Linear sweep voltammetry (LSV) and cyclic voltammetry (CV) were performed to evaluate HER performance. The glassy carbon electrode was polished to a mirror finish using alumina powder of 0.05 μm size and ultrasonically cleaned in distilled water for 10 min, followed by drying in an IR lamp. The electrolyte

DOI: 10.1021/acsomega.7b00678
ACS Omega 2017, 2, 7532−7545

solution was purged with N_2 gas for 30 min prior to the electrochemical measurements to remove dissolved oxygen. Before measurements, the samples were cycled at a scan rate of 10 mV s^{-1} 50 times to refresh the catalytic surface. All of the electrochemical measurements are reported against the potential versus reversible hydrogen electrode (RHE) as the reference electrode. The Ag/AgCl reference electrode was calibrated in a three-electrode system using a cleaned Pt electrode as the working electrode and Pt wire as the counter electrode. H_2SO_4 solution (0.5 M) was used as electrolyte which is purged using high purity H_2 gas before and during measurements. LSVs were recorded at the scan rate of 1 mV s^{-1}, and the potential where the current was zero is taken as the reference potential of the hydrogen electrode and was found to be −0.2246 V from Figure S8. All of the electrochemical potentials applied and measured using the Ag/AgCl reference electrode were converted to RHE using the following equation; in addition to conversion of the potential with respect to RHE, potentials were also corrected for the iR_s drop.

$$E_{corrected} = E_{Ag/AgCl} + 0.2246\ V - iR_s \quad (9)$$

where, $E_{Ag/AgCl}$ is the Ag/AgCl electrode potential, 0.2246 V is the corrected potential, R_s is the resistance of solution, iR_s is the potential drop due to solution resistance that is measured using electrochemical impedance measurements reported in the later section of this article.

All of the measurements were iR_s-compensated in the present study, and the values of R_s were found by conducting impedance measurement in 0.5 M H_2SO_4 and were in the range of 6−7 Ω for both MoS_2/GO and MoS_2/rGO composite materials. The temperature during electrochemical measurements was 25 ± 1°C. The overpotential "η" for hydrogen evolution was calculated using the following equation

$$\eta = E_{RHE} - 0\ V - 0.0591\ pH - iR_s \quad (10)$$

Atomic absorption spectrometry (AAS) was used for the chemical quantification of the catalyst; the Mo content was determined using the AAS instrument model Contra AA-300 from Analyticjena, Germany. The Mo content in both the samples were quantified at 20% (wt %). The presence of GO and rGO in the composite was determined by measuring the total carbon content in the sample using a carbon sulfur analyzer from Eltra. The GO and the rGO contents of the sample were kept the same, and the percentage composition of GO and rGO in the catalysts sample were determined at ∼60%.

■ ASSOCIATED CONTENT

Supporting Information

The Supporting Information is available free of charge on the ACS Publications website at DOI: 10.1021/acsomega.7b00678.

X-ray diffraction of pristine MoS_2; HRTEM images and the SAED pattern of MoS_2/GO nanocomposite materials; histogram of AFM of MoS_2/GO composite materials before and after the chronopotentiometry test; AFM images of MoS_2/rGO at two different resolutions; cyclic voltammetry of MoS_2/GO and MoS_2/rGO at different scan rates; cyclic voltammetry plots under hydrodynamic condition (at 1500 rpm) of MoS_2/GO and MoS_2/rGO; effect of temperature on the HER process for MoS_2/rGO catalyst and the Arrhenius plot; SECM images of MoS_2/rGO catalyst at different substrate potentials; linear sweep voltammetry (LSV) plot for calibration of the Ag/AgCl reference electrode with the RHE (PDF)

■ AUTHOR INFORMATION

Corresponding Author

*E-mail asatpati@barc.gov.in.

ORCID

Ashis Kumar Satpati: 0000-0002-2732-8706

Author Contributions

The manuscript was written through contributions of all authors. All authors have given approval to the final version of the manuscript.

Funding

This project is fully funded by our institute, Bhabha Atomic Research Centre, Government of India.

Notes

The authors declare no competing financial interest.

■ ACKNOWLEDGMENTS

We thank Dr. P.D. Naik, Associate Director Chemistry Group, Bhabha Atomic Research Centre, for his encouragements and support during the course of the present work.

■ ABBREVIATIONS

CV, cyclic voltammetry; LSV, linear sweep voltammetry; SEM, scanning electron microscope; TEM, transmission electron microscope; SAED, selected-area electron diffraction; HER, hydrogen evolution process; SECM, scanning electrochemical microscopy; RDE, rotating disk electrode; GC, glassy carbon; GO, graphene oxide; rGO, reduced graphene oxide; MoS_2, molybdenum sulfide; RHE, reversible hydrogen electrode; CPE, constant phase element

■ REFERENCES

(1) Xia, X. H.; Zhao, X. J.; Ye, W. C.; Wang, C. M. Highly porous Ag-Ag2S/MoS2 with additional active sites synthesized by chemical etching method for enhanced electrocatalytic hydrogen evolution. *Electrochim. Acta* **2014**, *142*, 173−181.

(2) Walter, M. G.; Warren, E. L.; McKone, J. R.; Boettcher, S. W.; Mi, Q.; Santori, E. A.; Lewis, N. S. Solar Water Splitting Cells. *Chem. Rev.* **2010**, *110*, 6446−6473.

(3) (a) Arenz, M.; Stamenkovic, V.; Schmidt, T. J.; Wandelt, K.; Ross, P. N.; Markovic, N. M. CO adsorption and kinetics on well-characterized Pd films on Pt(111) in alkaline solutions. *Surf. Sci.* **2002**, *506*, 287−296. (b) Elezović, N. R.; Gajić-Krstajić, L.; Radmilović, V.; Vračar, L.; Krstajić, N. V. Effect of chemisorbed carbon monoxide on Pt/C electrode on the mechanism of the hydrogen oxidation reaction. *Electrochim. Acta* **2009**, *54*, 1375−1382. (c) Fang, B.; Kim, J. H.; Yu, J.-S. Colloid-imprinted carbon with superb nanostructure as an efficient cathode electrocatalyst support in proton exchange membrane fuel cell. *Electrochem. Commun.* **2008**, *10*, 659−662. (d) Wu, Z.; Fang, B.; Bonakdarpour, A.; Sun, A.; Wilkinson, D.; et al. WS2 nanosheets as a highly efficient electrocatalyst for hydrogen evolution reaction. *Appl. Catal., B* **2012**, *125*, 59−66.

(4) (a) Hou, Y.; Zhang, B.; Wen, Z.; Cui, S.; Guo, X.; He, Z.; Chen, J. A 3D hybrid of layered MoS2/nitrogen-doped graphene nanosheet aerogels: an effective catalyst for hydrogen evolution in microbial electrolysis cells. *J. Mater. Chem. A* **2014**, *2*, 13795−13800. (b) Pan, L. F.; Li, Y. H.; Yang, S.; Liu, P. F.; Yu, M. Q.; Yang, H. G. Molybdenum carbide stabilized on graphene with high electrocatalytic activity for hydrogen evolution reaction. *Chem. Commun.* **2014**, *50*, 13135−13137. (c) Yan, Y.; Ge, X.; Liu, Z.; Wang, J. Y.; Lee, J. M.; Wang, X. Facile synthesis of low crystalline MoS2 nanosheet-coated CNTs for

DOI: 10.1021/acsomega.7b00678
ACS Omega 2017, 2, 7532−7545

enhanced hydrogen evolution reaction. *Nanoscale* **2013**, *5*, 7768−7771.
(5) (a) Merki, D.; Hu, X. Recent developments of molybdenum and tungsten sulfides as hydrogen evolution catalysts. *Energy Environ. Sci.* **2011**, *4*, 3878−3888. (b) Yan, Y.; Xia, B.; Xu, Z.; Wang, X. Recent development of molybdenum sulfides as advanced electrocatalysts for hydrogen evolution reaction. *ACS Catal.* **2014**, *4*, 1693−1705. (c) Lv, R.; Robinson, J. A.; Schaak, R. E.; Sun, D.; Sun, Y.; Mallouk, T. E.; Terrones, M. Transition metal dichalcogenides and beyond: synthesis, properties, and applications of single-and few-layer nanosheets. *Acc. Chem. Res.* **2015**, *48*, 56−64. (d) Li, Z.; Dai, X.; Du, K.; Ma, Y.; Liu, M.; Sun, H.; Ma, X.; Zhang, X. Reduced Graphene Oxide/O-MWCNT hybrids functionalized with p-Phenylenediamine as high-performance MoS2 electrocatalyst support for hydrogen evolution reaction. *J. Phys. Chem. C* **2016**, *120*, 1478−1487.
(6) (a) Ma, C. B.; Qi, X.; Chen, B.; Bao, S.; Yin, Z.; Wu, X. J.; Luo, Z.; Wei, J.; Zhang, H. L.; Zhang, H. MoS2 nanoflower-decorated reduced graphene oxide paper for high-performance hydrogen evolution reaction. *Nanoscale* **2014**, *6*, 5624−5629. (b) Zhang, K.; Zhao, Y.; Zhang, S.; Yu, H.; Chen, Y.; Gao, P.; Zhu, C. MoS2 nanosheet/Mo2C-embedded N-doped carbon nanotubes: synthesis and electrocatalytic hydrogen evolution performance. *J. Mater. Chem. A* **2014**, *2*, 18715−18719.
(7) (a) Li, Y.; Wang, H.; Xie, L.; Liang, Y.; Hong, G.; Dai, H. MoS2 nanoparticles grown on graphene: an advanced catalyst for hydrogen evolution reaction. *J. Am. Chem. Soc.* **2011**, *133*, 7296−7299. (b) Karunadasa, H. I.; Montalvo, E.; Sun, Y.; Majda, M.; Long, J. R.; Chang, C. J. A molecular MoS2 edge site mimic for catalytic hydrogen generation. *Science* **2012**, *335*, 698−702. (c) Chang, Y. H.; Lin, C. T.; Chen, T. Y.; Hsu, C. L.; Lee, Y. H.; Zhang, W.; Wei, K. H.; Li, L. J. Highly Efficient Electrocatalytic Hydrogen Production by MoSx Grown on Graphene-Protected 3D Ni Foams. *Adv. Mater.* **2013**, *25*, 756−760. (d) Xie, J.; Zhang, H.; Li, S.; Wang, R.; Sun, X.; Zhou, M.; Zhou, J.; Lou, X. W. D.; Xie, Y. Defect-rich MoS2 ultrathin nanosheets with additional active edge sites for enhanced electrocatalytic hydrogen evolution. *Adv. Mater.* **2013**, *25*, 5807−5813. (e) Tsai, C.; Abild-Pedersen, F.; Nørskov, J. K. Tuning the MoS2 edge-site activity for hydrogen evolution via support interactions. *Nano Lett.* **2014**, *14*, 1381−1387. (f) Tsai, C.; Chan, K.; Abild-Pedersen, F.; Nørskov, J. K. Active edge sites in MoSe 2 and WSe 2 catalysts for the hydrogen evolution reaction: a density functional study. *Phys. Chem. Chem. Phys.* **2014**, *16*, 13156−13164. (g) Benson, J.; Li, M.; Wang, S.; Wang, P.; Papakonstantinou, P. Electrocatalytic hydrogen evolution reaction on edges of a few layer molybdenum disulfide nanodots. *ACS Appl. Mater. Interfaces* **2015**, *7*, 14113−14122. (h) Gao, M. R.; Liang, J. X.; Zheng, Y. R.; Xu, Y. F.; Jiang, J.; Gao, Q.; Li, J.; Yu, S. H. An efficient molybdenum disulfide/cobalt diselenide hybrid catalyst for electrochemical hydrogen generation. *Nat. Commun.* **2015**, *6*, No. 5982.
(8) Merki, D.; Vrubel, H.; Rovelli, L.; Fierro, S.; Hu, X. Fe, Co, and Ni ions promote the catalytic activity of amorphous molybdenum sulfide films for hydrogen evolution. *Chem. Sci.* **2012**, *3*, 2515−2525.
(9) Shi, J.; Ma, D.; Han, G.-F.; Zhang, Y.; Ji, Q.; Gao, T.; Sun, J.; Song, X.; Li, C.; Zhang, Y.; Lang, X.-Y.; Zhang, Y.; Liu, Z. Controllable Growth and Transfer of Monolayer MoS2 on Au Foils and Its Potential Application in Hydrogen Evolution Reaction. *ACS Nano* **2014**, *8*, 10196−10204.
(10) Hinnemann, B.; Moses, P. G.; Bonde, J.; Jørgensen, K. P.; Nielsen, J. H.; Horch, S.; Chorkendorff, I.; Nørskov, J. K. Biomimetic Hydrogen Evolution: MoS2 Nanoparticles as Catalyst for Hydrogen Evolution. *J. Am. Chem. Soc.* **2005**, *127*, 5308−5309.
(11) Bonde, J.; Moses, P. G.; Jaramillo, T. F.; Norskov, J. K.; Chorkendorff, I. Hydrogen evolution on nano-particulate transition metal sulfides. *Faraday Discuss.* **2008**, *140*, 219−31 discussion 297−317..
(12) Jaramillo, T. F.; Bonde, J.; Zhang, J.; Ooi, B.-L.; Andersson, K.; Ulstrup, J.; Chorkendorff, I. Hydrogen evolution on supported incomplete cubane-type [Mo3S4] 4+ electrocatalysts. *J. Phys. Chem. C* **2008**, *112*, 17492−17498.
(13) (a) Lukowski, M. A.; Daniel, A. S.; Meng, F.; Forticaux, A.; Li, L.; Jin, S. Enhanced hydrogen evolution catalysis from chemically exfoliated metallic MoS2 nanosheets. *J. Am. Chem. Soc.* **2013**, *135*, 10274−10277. (b) Maitra, U.; Gupta, U.; De, M.; Datta, R.; Govindaraj, A.; Rao, C. Highly Effective Visible-Light-Induced H2 Generation by Single-Layer 1T-MoS2 and a Nanocomposite of Few-Layer 2H-MoS2 with Heavily Nitrogenated Graphene. *Angew. Chem., Int. Ed.* **2013**, *52*, 13057−13061. (c) Voiry, D.; Salehi, M.; Silva, R.; Fujita, T.; Chen, M.; Asefa, T.; Shenoy, V. B.; Eda, G.; Chhowalla, M. Conducting MoS2 nanosheets as catalysts for hydrogen evolution reaction. *Nano Lett.* **2013**, *13*, 6222−6227.
(14) (a) Allen, M. J.; Tung, V. C.; Kaner, R. B. Honeycomb Carbon: A Review of Graphene. *Chem. Rev.* **2010**, *110*, 132−145. (b) Chang, K.; Chen, W. L-Cysteine-Assisted Synthesis of Layered MoS2/Graphene Composites with Excellent Electrochemical Performances for Lithium Ion Batteries. *ACS Nano* **2011**, *5*, 4720−4728.
(15) Li, H.; Yu, K.; Li, C.; Tang, Z.; Guo, B.; Lei, X.; Fu, H.; Zhu, Z. Charge-Transfer Induced High Efficient Hydrogen Evolution of MoS2/graphene Cocatalyst. *Sci. Rep.* **2015**, *5*, No. 18730.
(16) (a) Acerce, M.; Voiry, D.; Chhowalla, M. Metallic 1T phase MoS2 nanosheets as supercapacitor electrode materials. *Nat. Nanotechnol.* **2015**, *10*, 313−318. (b) Bai, S.; Wang, L.; Chen, X.; Du, J.; Xiong, Y. Chemically exfoliated metallic MoS2 nanosheets: A promising supporting co-catalyst for enhancing the photocatalytic performance of TiO2 nanocrystals. *Nano Res.* **2015**, *8*, 175−183.
(17) (a) Coehoorn, R.; Haas, C.; Dijkstra, J.; Flipse, C.; De Groot, R.; Wold, A. Electronic structure of MoSe 2, MoS 2, and WSe 2. I. Band-structure calculations and photoelectron spectroscopy. *Phys. Rev. B: Condens. Matter Mater. Phys.* **1987**, *35*, 6195. (b) Coleman, J. N.; Lotya, M.; O'Neill, A.; Bergin, S. D.; King, P. J.; Khan, U.; Young, K.; Gaucher, A.; De, S.; Smith, R. J.; et al. Two-dimensional nanosheets produced by liquid exfoliation of layered materials. *Science* **2011**, *331*, 568−571. (c) Mak, K. F.; Lee, C.; Hone, J.; Shan, J.; Heinz, T. F. Atomically thin MoS 2: a new direct-gap semiconductor. *Phys. Rev. Lett.* **2010**, *105*, No. 136805.
(18) Li, H.; Zhang, Q.; Yap, C. C. R.; Tay, B. K.; Edwin, T. H. T.; Olivier, A.; Baillargeat, D. From bulk to monolayer MoS2: evolution of Raman scattering. *Adv. Funct. Mater.* **2012**, *22*, 1385−1390.
(19) Vargas C, O. A.; Caballero, Á; Morales, J. Can the performance of graphene nanosheets for lithium storage in Li-ion batteries be predicted? *Nanoscale* **2012**, *4*, 2083−2092.
(20) Zhang, J.; Zhao, L.; Liu, A.; Li, X.; Wu, H.; Lu, C. Three-dimensional MoS 2/rGO hydrogel with extremely high double-layer capacitance as active catalyst for hydrogen evolution reaction. *Electrochim. Acta* **2015**, *182*, 652−658.
(21) Huang, Y.; Nielsen, R. J.; Goddard, W. A., III; Soriaga, M. P. The reaction mechanism with free energy barriers for electrochemical dihydrogen evolution on MoS2. *J. Am. Chem. Soc.* **2015**, *137*, 6692−6698.
(22) Bard, A. J.; Faulkner, L. R. Fundamentals and Applications. In *Electrochemical Methods*, 2nd ed.; John Wiley & Sons: New York, 2001.
(23) McCrory, C. C.; Jung, S.; Ferrer, I. M.; Chatman, S. M.; Peters, J. C.; Jaramillo, T. F. Benchmarking hydrogen evolving reaction and oxygen evolving reaction electrocatalysts for solar water splitting devices. *J. Am. Chem. Soc.* **2015**, *137*, 4347−4357.
(24) Gasteiger, H. A.; Markovic, N. M.; Ross, P. N. H2 and CO Electrooxidation on Well-Characterized Pt, Ru, and Pt-Ru. 1. Rotating Disk Electrode Studies of the Pure Gases Including Temperature Effects. *J. Phys. Chem.* **1995**, *99*, 8290−8301.
(25) Yuan, X. Z.; Wang, H. PEM fuel cell fundamentals. In *PEM Fuel Cell Electrocatalysts and Catalyst Layers*; Springer, 2008; pp 1−87.
(26) Bard, A. J.; Parsons, R.; Jordan, J. *Standard Potentials in Aqueous Solution*; CRC Press, 1985; Vol. 6.
(27) (a) Swierk, J. R.; Klaus, S.; Trotochaud, L.; Bell, A. T.; Tilley, T. D. Electrochemical study of the energetics of the oxygen evolution reaction at nickel iron (oxy) hydroxide catalysts. *J. Phys. Chem. C* **2015**, *119*, 19022−19029. (b) Wu, G.; Li, N.; Zhou, D.-R.; Mitsuo, K.; Xu, B.-Q. Anodically electrodeposited Co + Ni mixed oxide electrode:

DOI: 10.1021/acsomega.7b00678
ACS Omega 2017, 2, 7532−7545

preparation and electrocatalytic activity for oxygen evolution in alkaline media. *J. Solid State Chem.* **2004**, *177*, 3682−3692.
(28) Conway, B.; Tilak, B. Interfacial processes involving electrocatalytic evolution and oxidation of H 2, and the role of chemisorbed H. *Electrochim. Acta* **2002**, *47*, 3571−3594.
(29) (a) Sheng, W.; Gasteiger, H. A.; Shao-Horn, Y. Hydrogen oxidation and evolution reaction kinetics on platinum: acid vs alkaline electrolytes. *J. Electrochem. Soc.* **2010**, *157*, B1529−B1536. (b) Pentland, N.; Bockris, J. M.; Sheldon, E. Hydrogen evolution reaction on copper, gold, molybdenum, palladium, rhodium, and iron mechanism and measurement technique under high purity conditions. *J. Electrochem. Soc.* **1957**, *104*, 182−194.
(30) (a) Benson, J.; Li, M.; Wang, S.; Wang, P.; Papakonstantinou, P. Electrocatalytic hydrogen evolution reaction on edges of a few layer molybdenum disulfide nanodots. *ACS Appl. Mater. Interfaces* **2015**, *7*, 14113−14122. (b) Li, Y.; Wang, H.; Xie, L.; Liang, Y.; Hong, G.; Dai, H. MoS2 nanoparticles grown on graphene: an advanced catalyst for the hydrogen evolution reaction. *J. Am. Chem. Soc.* **2011**, *133*, 7296−7299. (c) Lukowski, M. A.; Daniel, A. S.; Meng, F.; Forticaux, A.; Li, L.; Jin, S. Enhanced hydrogen evolution catalysis from chemically exfoliated metallic MoS2 nanosheets. *J. Am. Chem. Soc.* **2013**, *135*, 10274−10277. (d) Voiry, D.; Salehi, M.; Silva, R.; Fujita, T.; Chen, M.; Asefa, T.; Shenoy, V. B.; Eda, G.; Chhowalla, M. Conducting MoS2 nanosheets as catalysts for hydrogen evolution reaction. *Nano Lett.* **2013**, *13*, 6222−6227.
(31) (a) Dreyer, D. R.; Park, S.; Bielawski, C. W.; Ruoff, R. S. The chemistry of graphene oxide. *Chem. Soc. Rev.* **2010**, *39*, 228−240. (b) Gao, W.; Wu, G.; Janicke, M. T.; Cullen, D. A.; Mukundan, R.; Baldwin, J. K.; Brosha, E. L.; Galande, C.; Ajayan, P. M.; More, K. L.; et al. Ozonated graphene oxide film as a proton-exchange membrane. *Angew. Chem., Int. Ed.* **2014**, *53*, 3588−3593. (c) Szabó, T.; Tombácz, E.; Illés, E.; Dékány, I. Enhanced acidity and pH-dependent surface charge characterization of successively oxidized graphite oxides. *Carbon* **2006**, *44*, 537−545. (d) Vinothkannan, M.; Kannan, R.; Kim, A. R.; Kumar, G. G.; Nahm, K. S.; Yoo, D. J. Facile enhancement in proton conductivity of sulfonated poly (ether ether ketone) using functionalized graphene oxide—synthesis, characterization, and application towards proton exchange membrane fuel cells. *Colloid Polym. Sci.* **2016**, *294*, 1197−1207.
(32) Thangasamy, P.; Ilayaraja, N.; Jeyakumar, D.; Sathish, M. Electrochemical cycling and beyond: unrevealed activation of MoO 3 for electrochemical hydrogen evolution reactions. *Chem. Commun.* **2017**, *53*, 2245−2248.
(33) (a) Lu, X.; Lin, Y.; Dong, H.; Dai, W.; Chen, X.; Qu, X.; Zhang, X. One-step hydrothermal fabrication of three-dimensional MoS2 nanoflower using polypyrrole as template for efficient hydrogen evolution reaction. *Sci. Rep.* **2017**, *7*, 42309. (b) Metikoš-Huković, M.; Jukić, A. Correlation of electronic structure and catalytic activity of Zr−Ni amorphous alloys for the hydrogen evolution reaction. *Electrochim. Acta* **2000**, *45*, 4159−4170. (c) Zheng, Z.; Li, N.; Wang, C.-Q.; Li, D.-Y.; Zhu, Y.-M.; Wu, G. Ni−CeO 2 composite cathode material for hydrogen evolution reaction in alkaline electrolyte. *Int. J. Hydrogen Energy* **2012**, *37*, 13921−13932.
(34) Morin, S.; Dumont, H.; Conway, B. Evaluation of the effect of two-dimensional geometry of Pt single-crystal faces on the kinetics of upd of H using impedance spectroscopy. *J. Electroanal. Chem.* **1996**, *412*, 39−52.
(35) (a) Lyons, M. E.; Brandon, M. P. The significance of electrochemical impedance spectra recorded during active oxygen evolution for oxide covered Ni, Co and Fe electrodes in alkaline solution. *J. Electroanal. Chem.* **2009**, *631*, 62−70. (b) Conway, B.; Gileadi, E. Kinetic theory of pseudo-capacitance and electrode reactions at appreciable surface coverage. *Trans. Faraday Soc.* **1962**, *58*, 2493−2509.
(36) (a) Bard, A. J., Markin, M. V., Eds.; *Scanning Electrochemical Microscopy*; Marcel Dekker: New York, 2001. (b) Bard, A. J.; Fan, F. R. F.; Kwak, J.; Lev, O. Scanning electrochemical microscopy. Introduction and principles. *Anal. Chem.* **1989**, *61*, 132−138.
(37) Li, H.; Du, M.; Mleczko, M. J.; Koh, A. L.; Nishi, Y.; Pop, E.; Bard, A. J.; Zheng, X. Kinetic study of hydrogen evolution reaction over strained MoS2 with sulfur vacancies using scanning electrochemical microscopy. *J. Am. Chem. Soc.* **2016**, *138*, 5123−5129.
(38) Ahn, H. S.; Bard, A. J. Electrochemical Surface Interrogation of a MoS2 Hydrogen-Evolving Catalyst: In Situ Determination of the Surface Hydride Coverage and the Hydrogen Evolution Kinetics. *J. Phys. Chem. Lett.* **2016**, *7*, 2748−2752.
(39) (a) Tang, Q.; Jiang, D.-e. Mechanism of hydrogen evolution reaction on 1T-MoS2 from first principles. *ACS Catal.* **2016**, *6*, 4953−4961. (b) Yang, J.; Wang, K.; Zhu, J.; Zhang, C.; Liu, T. Self-Templated Growth of Vertically Aligned 2H-1T MoS2 for Efficient Electrocatalytic Hydrogen Evolution. *ACS Appl. Mater. Interfaces* **2016**, *8*, 31702−31708.
(40) (a) Ma, Q.; Zhu, X.; Zhang, D.; Liu, S. Graphene oxide - a surprisingly good nucleation seed and adhesion promotion agent for one-step ZnO lithography and optoelectronic applications. *J. Mater. Chem. C* **2014**, *2*, 8956−8961. (b) Zhang, D.; Ma, Q.; Fan, H.; Yang, H.; Liu, S. F. Millimeter-long multilayer graphene nanoribbons prepared by wet chemical processing. *Carbon* **2014**, *71*, 120−126.

DOI: 10.1021/acsomega.7b00678
ACS Omega 2017, 2, 7532−7545